

## REDUCED POWER LOSS AND CONTROLLED TECHNIQUE FOR WIRELESS PTS USING CONTROLLERS

**K G GOVINDRAO, S.Bharath , D.Rahul Naik, K.Maniteja, V.Saikethan Reddy**  
 Assist. Prof. Dept. Of EEE TKR College of Engineering & Technology (Autonomous), Affiliated to JNTUH Hyderabad,India.  
 ,B.Tech student,EEE, TKR College of Engineering & Technology (Autonomous), Affiliated to JNTUH Hyderabad, India.  
 B.Tech student,EEE, TKR College of Engineering & Technology(Autonomous), Affiliated to JNTUH Hyderabad,India.  
 B.Tech student,EEE,TKR College of Engineering & Technology (Autonomous), Affiliated to JNTUH Hyderabad,India.  
 B.Tech student,EEE, TKR College of Engineering & Technology (Autonomous), Affiliated to JNTUH Hyderabad,India.

### ABSTRACT

Electric vehicles with different output power levels can use wireless power transfer (WPT) systems. Different vehicle assemblies (VAs) may be charged by different ground assemblies (GAs) in charging stations. However, the overall efficiency of the WPT system may drop significantly when the power class difference between GA and VA is large. To address this issue this article proposes a dc-link parallel ac-link series multi-inverter multi rectifier architecture for high-power WPT systems. Modulation, power transfer capability, and power sharing from the design aspects are investigated. A detailed power loss analysis and an easy-to-implemented power loss optimized control method based on mutual inductance

identification are presented in this article. Finally, experimental results are obtained from a 20-kW LCC-LCC WPT system to validate the analysis and proposed system operation.

### I.INTRODUCTION

WIRELESS power transfer (WPT) can achieve automatic charging for electric vehicles (EVs) without user intervention which provides a better user experience than

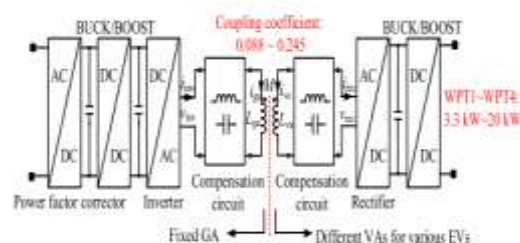


**Fig. 1.1 Diagram of the conventional EV WPT system.**

Fig 1 shows the conventional diagram of EV WPT system, conventional plug-in chargers. In recent years, academic research, industrial products, and international standards have been conducted, looking at optimal control methods, coil and circuit design, and power and efficiency improvements. Fig. 1 shows the diagram of the EV WPT system which consists of the ground assembly (GA) and the vehicle assembly (VA). The power is supplied from the grid and a power factor corrector (PFC) turns the mains ac voltage into a stable dc voltage. DC/DC converters such as buck/boost can be added to the GA and VA to obtain a wide range of power regulations. Series, parallel, and compound circuits have been proposed to compensate for the reactance of the coils, and the LCC-LCC compensation circuit is widely used for EV WPT products +.

Due to the large range of the battery capacities in different EVs and variables such as the parking positions, power rating and

coupling coefficient of the EV WPT system can change considerably. According to the definition of the international wireless charging standard SAE J2954 in the output power ratings range from 3.3 kW to higher than 20 kW, and the coupling coefficient can range from 0.088 to 0.245. Although multiple transmitter (Tx) coils, multiple receiver (Rx) coils, and multiple cells are conducive to power level improvement original equipment manufacturers have strict restrictions on the size, weight, and cost of the GA and VA. For example, manufacturers like Hongqi for their E-HS9 model require the 10-kW VA to be less than  $37\text{ cm} \times 37\text{ cm} \times 6\text{ cm}$  and weigh less than 17 kg. The required offsets defined in SAE J2954 are  $\pm 75\text{ mm}$  on the X-axis and  $\pm 100\text{ mm}$  on the Y-axis. Since Tx coils larger than RX coils result in improved misalignment tolerance caused by different parking positions, the EV WPT system usually has a large Tx coil and a small Rx coil (one-to-one coil design). Considering the cost and the limited volume of

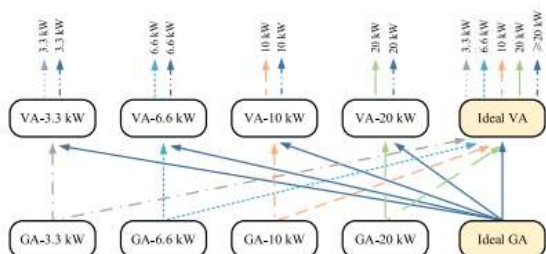


**Fig. 1.2. Interoperability of different GAs and VAs in charging stations.**

EVs, the high-power WPT system with one Tx coil and RX coil is more practical and has already been adopted by the EV WPT suppliers like WiTricity, ZTE, VIE, etc. Currently, the design of a WPT system usually provides customized parameters for different power ratings and power transfer distances. Various dc/dc converters active rectifiers phase-shifted capacitors and variable inductors have been proposed to achieve a wide output power range with a large coupling coefficient variation. In addition, different modulation schemes have been investigated including duty cycle control phase shift control frequency shift control pulse density modulation and ON-OFF keying. Research reported in and shows

the design of 50-kW and 100-kW coupling coils with a dc/dc efficiency higher than 95.5% under 160 mm power transfer distance, respectively.

The customized WPT system has already achieved high efficiency and high power. However, this design of GA and VA is only feasible for domestic use where the interoperability is not considered. A GA used as a public facility needs to be compatible with different VAs as shown in Fig. 2. When the GA and VA with different power ratings operate with each other, the equivalent impedance of the resonant tank deviates from the optimal region. This may result in a significant decrease in the output power and overall efficiency. For example, a 20-kW GA interoperating with a 20-kW VA should be able to deliver 20 kW efficiently, while the same GA interoperating with a 3.3-kW VA is also able to deliver 3.3 kW but with a significant loss in efficiency caused by impedance mismatch. As defined in SAE J2954 for interoperability, the overall efficiency decreases with the increase of the power

class difference and it is only 75% when two power class difference exists. Since the industrialization of wireless charging technology for EVs is advancing rapidly,

The interoperability requirement is becoming increasingly important, especially for the high-power WPT systems used in charging stations. In high-frequency and high-power WPT systems, power loss optimized control (PLOC) is important where heat dissipation would otherwise become difficult.

The buck/boost converters or active rectifiers are used to regulate the inverting and rectifying voltages against system parameter variations through traversing algorithms, simulated annealing algorithms, perturbation and observation (P&O) algorithms, and online parameter identification algorithms. However, these additional circuits are difficult to achieve wide-range soft switching under all operating conditions. The switching power losses of these converters increase when hard switching occurs.

In addition, these additional circuits increase the size and cost of the overall system. For the interoperability of the EV WPT systems with different power levels, a PLOC method is required to maximize the power transfer capability of the system to reduce the charging time and to obtain a high efficiency to ensure good heat dissipation simultaneously.

In summary, there is relatively little literature on the interoperability of the EV WPT systems, and no comprehensive design guidelines and control algorithms are available that simultaneously optimize both the power transfer capability and overall efficiency, especially for public wireless charging stations. The essential requirement for strong interoperability is that both GA and VA need to have strong power regulation abilities under soft-switching conditions.

However, dual-side dc/dc converters increase the number of cascaded main circuits which may decrease power density and increase costs, and complex high-frequency synchronization of active rectifiers or

phaseshifted capacitors reduces the charging reliability. To solve this problem, a dc-link parallel ac-link series (DPAS) multi-inverter multirectifier (MIMR) architecture is proposed in this article, whose contributions can be summarized as follows.

- 1) A modular DPAS-MIMR architecture with strong interoperability for the high-power WPT system used in charging stations.
- 2) A novel mutual inductance identification-based easy-to-implemented PLOC method.
- 3) Experimental validation of a 20-kW efficient, high-power, and flexible EV WPT system.

The remainder of this article is structured as follows. Section II introduces the proposed DPAS-MIMR WPT system and examines its modulation strategies, power transfer performance, and power sharing mechanisms. In Section III, the analysis of power losses is presented, along with efficiency optimization methods under varying coupling coefficients and output power conditions. Section IV details a

simplified PLOC approach that achieves both high efficiency and reduced system complexity. Experimental results validating the proposed system are provided in Section V. Finally, Section VI offers the conclusions of this study.

## II. LITERATURE SURVEY

[1]Liu et al. (2022) developed a capacitive power transfer system employing a double T-type resonant network, aimed at enhancing charging and power supply efficiency for mobile devices. Similarly,[2] Fan et al. (2021) investigated the combination of wireless power transfer with full-duplex communication using a shared coupling interface, demonstrating the feasibility of concurrent power and data transmission. In another study,

[3]Hou et al. (2021) proposed an innovative analysis approach based on the quadratic eigenvalue problem to optimize multi-relay magnetic coupling in wireless power transfer, leading to improved system performance earlier, Covic and Boys (2013) provided an overview of advancements in inductive

power transfer systems, particularly highlighting their applications in transportation.

Chopra and Bauer [4](2013) presented a case study focused on enhancing the driving range of electric vehicles through the use of on-road, contactless power transfer systems. In related research, [5] Chen et al. (2015) examined double-coupled inductive power transfer systems designed for roadway applications, contributing to the advancement of wireless charging solutions for electric vehicle fleets.

[6] Li and Mi (2015) concentrated on wireless power transfer technologies tailored for electric vehicle applications, proposing scalable and efficient methods to support the broader adoption of EV systems. [7] Song et al. (2021) explored a narrow-rail, three-phase magnetic coupler designed for dynamic wireless charging, which enhanced the consistency of output power supplied to electric vehicles.

[8] Choi et al. (2015) reviewed progress in wireless power transfer technologies aimed at

roadway-powered electric vehicles, presenting multiple strategies to improve overall system performance [9]. Wang et al. (2018) introduced a novel magnetic coupling design for dynamic wireless charging of electric vehicles, which boosts efficiency even under variable coupling conditions. In another domain, Can et al. (2021) engineered a lightweight, surface-conforming magnetic coupler for wireless charging of autonomous underwater vehicles, optimizing magnetic coupling in aquatic environments.

[11] Lu et al. (2020) introduced a high-efficiency, long-distance power relay system that ensures uniform power distribution, enabling stable energy transfer over extended ranges. In a subsequent work, [12] Lu et al. (2021) investigated the design and performance of an omnidirectional, dual-band wireless power transfer system capable of operating effectively across multiple frequency bands for enhanced efficiency. Additionally, [13] Tan et al. (2020) concentrated on optimizing power stability in three-dimensional wireless power transmission systems serving multiple loads,

proposing methods to strengthen overall system reliability

[14]Ha-Van et al. (2022) developed a cylindrical transmitting coil designed for two-dimensional omnidirectional wireless power transfer, significantly enhancing the efficiency of energy delivery. [15] Yan et al. (2022) proposed a multi-load wireless power transfer system featuring a concentrated magnetic field, specifically designed to optimize energy distribution in Autonomous Underwater Vehicle (AUV) cluster systems. Additionally,[16] Yang et al. (2022) presented an undersea system that enables both wireless power and data transfer, utilizing marine renewable energy to provide a sustainable solution for underwater operations

[17]Chen et al. (2019) developed a wireless system for both power and data transmission tailored for submarine cable-inspection robotic fish, utilizing a time-sharing multiplexing strategy to enhance the efficiency of communication and energy transfer. [18]Wu et al. (2015) proposed a

combined wireless power and data transfer solution employing a shared inductive link and frequency division multiplexing, thereby improving the simultaneous transfer performance.Furthering this field, Wu et al. (2020) presented a system for simultaneous wireless information and power transmission, featuring separate channels for data transfer to enhance system adaptability

[19] Cha et al. (2021) designed an innovative magnetic structure to enable omnidirectional wireless power transfer, contributing to more versatile and efficient system designs.optimized a three-coil, long-range, and dimension-asymmetric wireless power transfer system, focusing on enhancing both range and application flexibility

### III. PROPOSED DPAS-MIMR WPT SYSTEM

This section presents the proposed DPAS-MIMR WPT system and its synchronization principle. In addition, the power transfer capability and power-sharing

characteristics of the proposed DPAS-MIMR WPT system are discussed.

## A. Proposed Topology

The structure of the proposed system is illustrated in Fig. 3. Here,  $V_{bus}$  and  $V_{bat}$  represent the input and output DC-link voltages, respectively. The parameters  $m$  and  $n$  denote the number of inverters and rectifiers in the system. The inverter is built using MOSFETs labeled  $S_{1i}$  to  $S_{4i}$ , while the rectifier stage includes MOSFETs  $Q_{1j}$  and  $Q_{2j}$  along with diodes  $D_{1j}$  and  $D_{2j}$ . The resonant voltage and current on the inverter side are denoted as  $v_{pi}$  and  $i_{pi}$  while  $v_{sj}$  and  $i_{sj}$  represent the resonant voltage and current on the rectifier side. A DC blocking capacitor,  $C_b$  is included, which must have a low capacitive reactance (below  $0.5 \Omega$ ) and be capable of handling high inverter current at 85 kHz. When symmetrical phase shift control is applied, no DC component appears in  $v_{pi}$  ensuring proper operation of  $C_b$ .

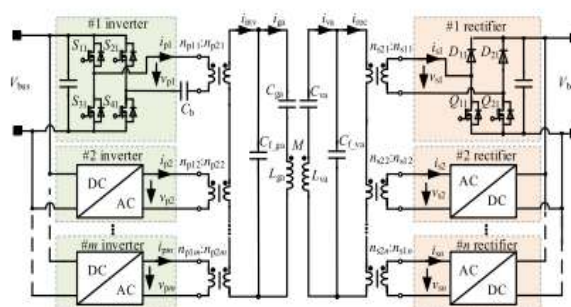


**Fig. 3.1 Proposed DPAS-MIMR WPT system.**

However, the regulation range is limited and hard switching occurs when the phase shift angle is large. Hence, an asymmetric control method is proposed and the half-bridge mode is introduced. Since there exists a dc component in this mode, a dc-blocking capacitor is required.

DC-blocking capacitors can be placed on all inverters and rectifiers; however, to minimize the total number of these components, a single capacitor on the inverter side is sufficient. This setup also supports the use of asymmetric modulation methods, such as half-bridge duty cycle control. With multiple inverters and active rectifiers in operation, synchronization

among controllers becomes essential. In this work, the inverter functions as the master unit, producing a square-wave synchronization signal, while the other inverters operate as slaves. The compensation capacitors in the LCC-LCC network are labeled as  $C_{f\_ga}$ ,  $C_{ga}$ ,  $C_{va}$  and  $C_{f\_va}$ . The inductive elements of the coupling coils are denoted by  $L_{ga}$  and  $L_{va}$ . The terms  $np1i$  ( $ns1i$ ) and  $np2i$  ( $ns2i$ ) represent the numbers of turns in the primary and secondary windings of the resonant inductor-integrated transformers (RIITs) on the ground assembly (GA) and vehicle assembly (VA), respectively, with their turns ratios designated as  $m_i$  and  $n_j$ .

Equivalent circuit of the proposed DPAS-MIMR WPT system is illustrated. In this configuration,  $R_{p1i}$  and  $R_{p2i}$  represent the primary and secondary parasitic resistances of the  $i$ -th RIIT on the ground assembly (GA), respectively. Similarly,  $R_{s1j}$  and  $R_{s2j}$  correspond to the primary and secondary parasitic resistances of the  $j$ -th RIIT on the vehicle assembly (VA). The parasitic resistances of the coupling coils are

denoted by  $R_{ga}$  and  $R_{va}$ . Additionally,  $R_{f\_ga}$  and  $R_{f\_va}$  indicate the total equivalent parasitic resistances associated with the DPAS-based inverters and rectifiers, respectively. The leakage inductances of the  $i$ -th and  $j$ -th RIITs on the GA and VA sides are labeled as  $L_{f\_gai}$  and  $L_{f\_vaj}$ , respectively.

Even though using a sandwich structure can minimize leakage inductance, additional resonant inductors are still required. To lower both the size and cost of the system, the leakage inductance inherent in the RIITs is utilized as the resonant inductance. The overall reactance can be calculated similarly to the traditional LCC-LCC topology, with an accuracy margin of around 5%. Therefore, the total leakage inductance can be effectively determined using this approach.

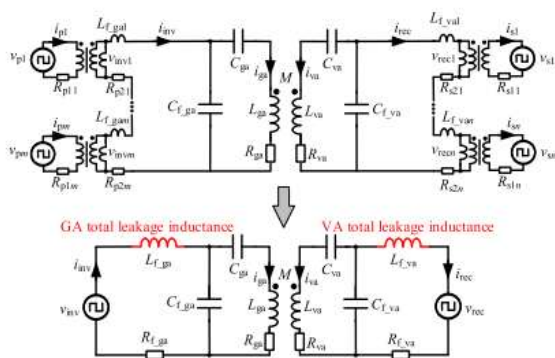


**Fig. 3.2. Equivalent circuit of the proposed DPAS-MIMR WPT system.**

The secondary windings of the RIITs are connected in series. Here,  $v_{inv}$  represents the secondary voltage of the RIIT on the ground assembly (GA), while  $v_{rec}$  denotes the secondary voltage of the RIIT on the vehicle assembly (VA). By summing these values, the total inverter-side voltage ( $v_{inv}$ ) and rectifier-side voltage ( $v_{rec}$ ) can be determined

## B. Power Transfer Analysis

The power rating of the proposed topology can be expanded by adding more cells. In addition, it can adapt to large variations in coupling coefficient, output power, and battery voltage.

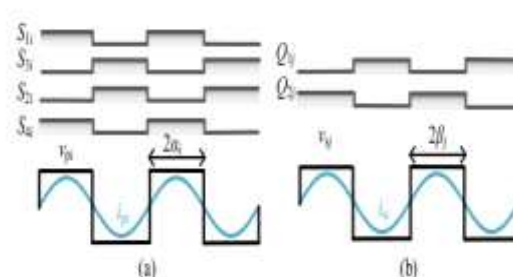


**Fig. 3.3 Typical waveforms of phase shift control. (a) Waveforms of inverter; (b) Waveforms of rectifier.**

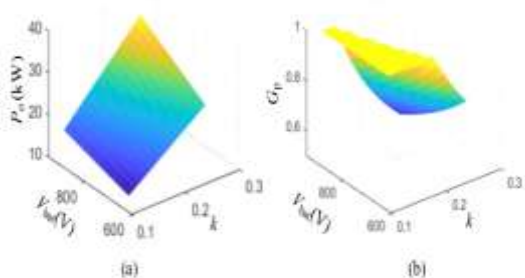
This section explains the modulation strategies used in the proposed topology, presents the power transfer analysis, and discusses how the system adapts to variations in key parameters. As illustrated in Fig. 5, the modulation schemes for both the inverters and rectifiers are synchronized. Phase shift control is applied, with phase angles represented by  $\alpha_i$  for the inverters and  $\beta_j$  for the rectifiers. Increasing  $\alpha_i$  and  $\beta_j$  facilitates soft switching in both stages. Due to the effective filtering characteristics of the LCC resonant circuit, fundamental harmonic analysis (FHA) is commonly employed in WPT systems. Power transfer is primarily influenced by the fundamental harmonic

components of voltage, whose RMS values can be calculated accordingly. To minimize reactive power, the system is designed to operate at its resonant frequency. The output power ( $P_o$ ) can be approximated under this condition. Additionally, to alleviate voltage regulation stress on the inverter and rectifier stages, a front-end power factor correction (PFC) unit is included for voltage stabilization. Here,  $\lambda$  and  $V_{bus\_max}$  denote the voltage ratio and the maximum allowable  $V_{bus}$ , respectively.

The inverters and receivers are synchronized with each other to maximize the power transfer capability. One can obtain the output power  $P_o$

**Fig.3.4 3-D Plots of  $P_{ref}$  and  $G_p$  concerning  $k$  and  $p_o$  with diode rectifiers for a 20 kw WPT system**

$P_{ref}$  serves as the fundamental unit that defines the power transfer capability of the DPAS-MIMR WPT system. By increasing the values of  $m$  and  $n$ , which together determine  $G_p$ , the system's power rating can be scaled up. As indicated, selecting appropriate values for  $m$ ,  $n$ ,  $m_p$ , and  $n_s$  is critical. The parameters  $m$  and  $n$  are chosen based on the individual power capacity of each converter and the total power output required. For instance, if one inverter and one rectifier can handle 10 kW—depending on the semiconductor devices used and the cooling efficiency—then setting  $m$  and  $n$  to 2 would allow the system to achieve 20 kW. Furthermore, the values for  $m_p$  and  $n_s$  are selected based on constraints such as the maximum allowable resonant currents ( $I_{ga\_max}$  and  $I_{va\_max}$ ), as well as the peak input and output voltages ( $V_{bus\_max}$  and  $V_{bat\_max}$ ).



In practical applications, designers must take into account the limitations of both the output charging current and voltage. The battery voltage ( $V_{bat}$ ) fluctuates depending on its state of charge, while the charging current is defined by the target power level. Additionally, the coupling coefficient ( $k$ ) changes with vehicle parking alignment. For example, if  $V_{bat}$  and  $k$  vary within the ranges of 650 V to 920 V and 0.14 to 0.26, respectively, and the required output power is set at 20 kW, the peak charging current would be approximately 30.8 A.

A. Fig. 6 shows the 3D plot of  $P_{ref}$  and  $G_p$  concerning  $V_{bat}$  and  $k$  for a 20-kW WPT system where  $I_{ga\_max} = 65$  Arms and  $I_{va\_max} = 55$  Arms determined by system heat dissipation capability.  $P_{ref}$  increases with  $V_{bat}$  and  $k$ , and a higher  $P_{ref}$  corresponds to a stronger power transfer capability of the coils. When both  $V_{bat}$  and  $k$  are small,  $P_{ref}$  is smaller than 20 kW where  $G_p$  is set at 1. When both  $V_{bat}$  and  $k$  are maximum,  $P_{ref}$  approaches 37.4 kW where  $G_p$  should be set at the minimum value (0.54) to limit the output power to 20 kW. Although

$V_{bat}$  and  $k$  vary, one can design proper  $m$ ,  $n$ ,  $m_p$ ,  $n_s$ ,  $\alpha_i$ ,  $\beta_j$ , and  $\lambda$  to achieve different  $G_p$ . Therefore, the proposed DPAS-MIMR architecture has strong interoperability and can adapt to various VAs with different power ratings.

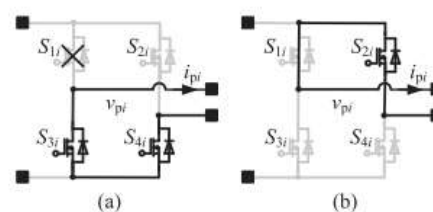


**Fig. 3.5 FMEA of inverter. (a) Open-circuited fault. (b) Short-circuited fault.**

## D. Failure Mode And Effect Analysis

Ensuring reliability is crucial in MIMR systems, as the use of a larger number of power semiconductor components can potentially raise the system's failure rate. To address this, a failure mode and effect analysis (FMEA) is carried out for the multiple inverters in the DPAS-MIMR configuration. Power semiconductor devices are prone to faults, which typically manifest as either open-circuit or short-circuit

conditions. Figures 7(a) and 7(b) illustrate these fault scenarios in a full-bridge inverter, showing the cases of open-circuit and short-circuit failures, respectively.

If  $S1i$  experiences an open-circuit fault, then  $S3i$  and  $S4i$  remain continuously on, while  $S2i$  stays off. In this condition, inverter #i is effectively bypassed, allowing the remaining inverters to continue operating normally. In the case where  $S1i$  is short-circuited,  $S3i$  and  $S4i$  are turned off, and  $S2i$  is kept permanently on. This same fault-handling approach can be applied to similar failures in the other MOSFETs. As a result, only the faulty inverter (#i) is bypassed, and the rest of the inverters maintain normal operation. Consequently, the power transfer capability of the system is reduced by only  $1/m$  when a single semiconductor failure occurs in one inverter. The greater the value of  $m$ , the less significant the effect of such faults on overall system performance.

## IV. MATLAB RESULTS ANALYSIS

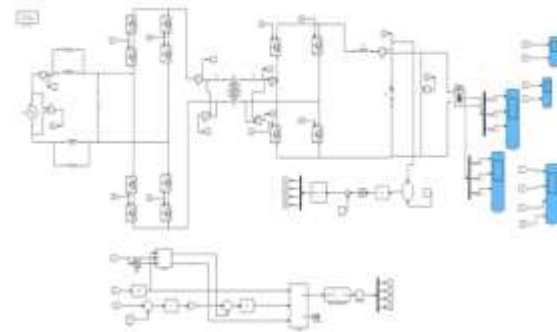


**Fig 4.1 illustration of pi controller**

The above circuit diagram illustrates a wireless power transfer (WPT) system designed in MATLAB Simulink, incorporating a Proportional-Integral (PI) controller for regulating output parameters. The setup includes a power source connected to a full-bridge inverter, which converts DC to high-frequency AC for efficient inductive coupling. The inverter is followed by a compensation network and a pair of loosely coupled coils that enable wireless energy transmission. On the receiver side, the induced AC voltage is rectified and filtered to produce a stable DC output. The PI controller monitors key variables such as output voltage or current and dynamically adjusts the inverter switching to maintain stable

operation and improve power transfer efficiency. Feedback signals are processed and fed into the controller, which helps minimize steady-state error and improve dynamic response. The scope blocks at the right end are used for monitoring critical system waveforms such as voltage, current, and control signals during simulation.

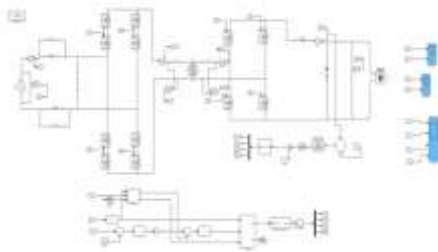


**fig 4.2 illustrationof fuzzy controller**

The Simulink-based wireless power transfer (WPT) system is designed for electric vehicle applications, combining solar photovoltaic (PV) input, a hybrid battery backup, and a motor drive unit. The system starts with ac supply from grid and an auxiliary source, which is regulated through DC-DC converters to maintain stable voltage levels. A full-bridge inverter converts the regulated DC into high-frequency AC, which

is then transmitted wirelessly using inductive coupling enhanced by a resonant LC circuit for efficient energy transfer. On the receiving end, the AC signal is rectified back to DC and managed for charging a backup battery. The motor drive section includes a speed-controlled STM motor managed through a PID controller and PWM signals, ensuring smooth operation under different load conditions. Additionally, a hybrid power management system intelligently switches between solar and battery power, ensuring uninterrupted operation. The circuit also includes monitoring blocks to track key parameters like voltage, current, and motor performance, making it a reliable and efficient solution for contactless energy delivery in EV and hybrid systems.

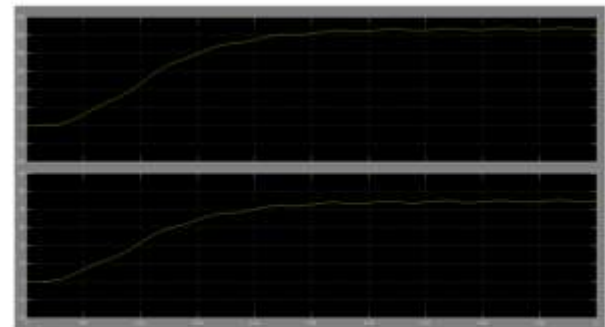


**fig:4.3 vdc and idc outputs**

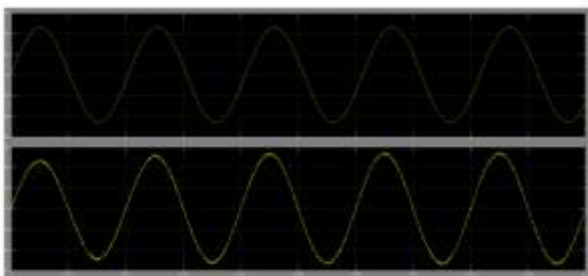


**fig 4.4. grid voltage and current outputs**

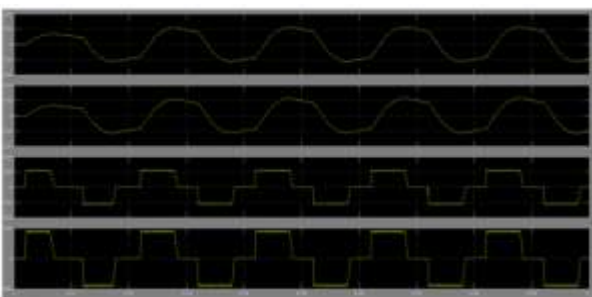


**fig 4.5. primary and secondary current and voltages**

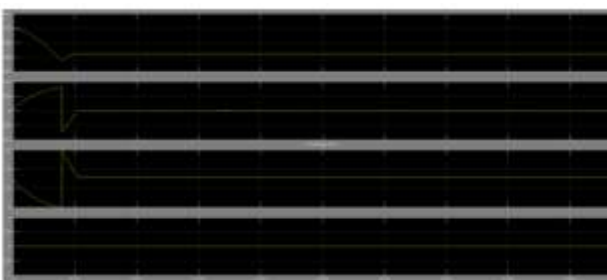


**Fig-4.6. battery performance**

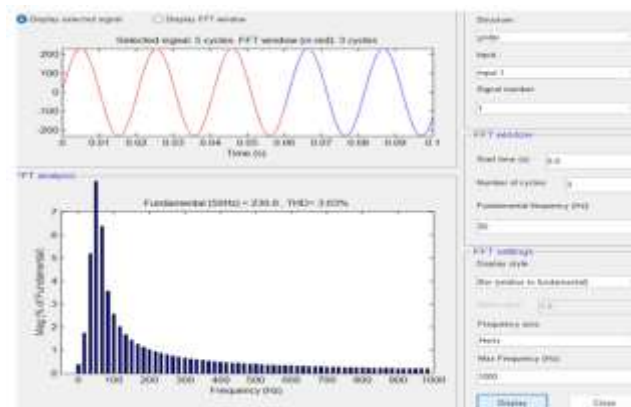


**fig 4.7 graph of gridpi**

The figure above illustrates a total harmonic distortion of 3.63% when the power supply is sourced from the grid, which impacts the power transfer efficiency.

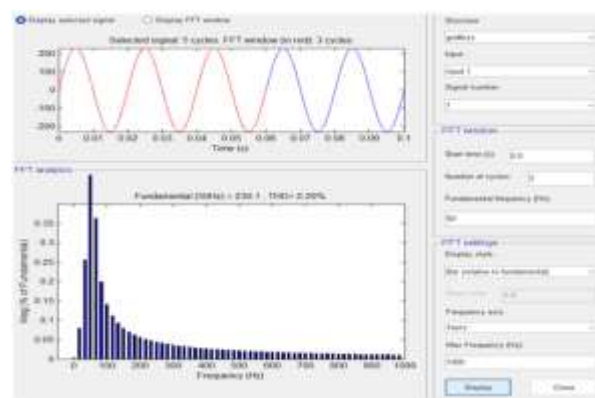


**fig 4.8 graph of grid fuzzy**

The figure above demonstrates a reduction in total harmonic distortion to 0.20% by employing fuzzy logic and PI

controllers compared to the grid supply. This decrease in distortion results in reduced power losses and an increase in power transfer efficiency between the two assemblies.

## CONCLUSION

This paper introduces a DPAS-MIMR architecture to enhance the power efficiency and interoperability of EV wireless power transfer (WPT) systems. Additionally, a simplified PLOC method based on mutual inductance identification is proposed to reduce power losses under varying coupling coefficients and power fluctuations. By eliminating conventional dc/dc regulators and resonant inductors in the LCC-LCC compensation circuit, the system achieves greater efficiency. The topology's inherent characteristics enable power sharing among converters without the need for complex closed-loop controls. This system is efficient, cost-effective, compact, and offers strong interoperability, making it ideal for industrial EV WPT applications. A 20-kW WPT platform with two inverters and two rectifiers

has been developed, achieving a maximum overall efficiency of 95%. Even with variations in output power (from 2.8 kW to 20 kW), battery voltage (from 650 V to 915 V), and coupling coefficient (from 0.155 to 0.26), the system maintains a minimum efficiency exceeding 88%.

## REFERENCES

1. H. Hu, S. Lyu, C. Zhao, Y. Su, and C. Ma, "Multiple Loop Coil Switching Technique for Wireless Power Transfer System with Fixed Frequency and Fixed Duty Ratio," *Energies*, vol. 9, no. 3, pp. 156, Mar. 2016. [Online]. Available: <https://www.mdpi.com/1996-1073/9/3/156>
2. H. Ju and R. Zhang, "A Voting-Based Distributed Charging Control in Broadband Wireless Power Transfer Networks," *arXiv preprint arXiv:1608.04466*, 2016. [Online]. Available: <https://arxiv.org/abs/1608.04466>

3. D. Yang, Y. Liu, Z. Cheng, and L. Zhang, "Phase Difference Control of Coil Currents in Wireless Power Transfer Systems to Reduce Leakage Magnetic Fields," *Energies*, vol. 15, no. 21, pp. 8202, Nov. 2022. [Online]. Available: <https://www.mdpi.com/1996-1073/15/21/8202>
4. S. T. Lee, J. C. Park, and D. H. Lee, "Frequency Tracking Control of Resonant WPT System with Fixed Switching Frequency," *Journal of Physics: Conference Series*, vol. 2108, no. 1, pp. 012023, 2021. [Online]. Available: <https://iopscience.iop.org/article/10.1088/1742-6596/2108/1/012023>
5. X. Yang, Y. Wang, L. Ma, and W. Liu, "A High-Frequency Wireless Power Transfer System with Self-Adaptive Voltage Stabilization Control," *IET Power Electronics*, vol. 13, no. 18, pp. 4013–4022, Dec. 2020. [Online]. Available: <https://ietresearch.onlinelibrary.wiley.com/doi/full/10.1049/iet-pel.2019.0931>
6. A. Magno, D. Singh, J. Anastasova, and K. Yang, "Controlled Resonance Tuning for Wireless Power Transfer to Miniature Telemetric Devices," *Wireless Power Transfer*, vol. 7, e1, 2020. [Online]. Available: <https://www.maxapress.com/article/doi/10.1017/wpt.2020.1>
7. J. Liu, M. Zhang, and Z. Zhao, "A Closed-Loop Control of Laser-Based Wireless Power Transfer System with Improved Efficiency," *IET Power Electronics*, vol. 13, no. 17, pp. 3855–3862, Nov. 2020. [Online]. Available: <https://ietresearch.onlinelibrary.wiley.com/doi/10.1049/iet-pel.2019.1372>
8. B. Clerckx, R. Zhang, R. Schober, D. W. K. Ng, D. I. Kim, and H. V. Poor, "Fundamentals of Wireless Information and Power Transfer: From RF Energy Harvester Models to Signal and System Designs," *IEEE Journal on Selected Areas in Communications*, vol. 37, no. 1,

pp. 4–33, Jan. 2019. [Online]. Available:  
<https://arxiv.org/abs/1501.02429>

9. S. Ichikawa, Y. Aoyagi, and T. Yamamoto, "Control Method of a Three-Phase Wireless Power Transfer System under Misalignment Conditions," *IEEJ Journal of Industry Applications*, vol. 9, no. 4, pp. 401–409, Jul. 2020. [Online]. Available:  
[https://www.jstage.jst.go.jp/article/ieejjia/9/4/9\\_401/\\_article](https://www.jstage.jst.go.jp/article/ieejjia/9/4/9_401/_article)

10. Y. Li, J. Wang, and K. Wu, "A Switched-Capacitor-Assisted Wireless Power Transfer System with Global Control and Local Regulation," *Electronics Letters*, vol. 56, no. 10, pp. 497–499, May 2020. [Online]. Available:  
<https://ietresearch.onlinelibrary.wiley.com/doi/full/10.1049/ell2.12496>



**K G GOVINDRAO (M.Tech (P.E))**

Completed B.E in Electrical & Electronics Engineering in 2014 from BLDEA's Engg College and Tech Vijayapura affiliated to VTU Belagavi, KARNATAKA and M.Tech in Power Electronics in 2018, from Ballari institute of Technology and management Engineering College Affiliated to VTU, Belagavi, Karnataka, India. Area of interest includes Power Electronics, Electrical Drive control and Multilevel inverters.

E-mail id: [govindkulkarni719@gmail.com](mailto:govindkulkarni719@gmail.com)